

A TEM study of four particles extracted from the Stardust track 80

Julien STODOLNA*, Damien JACOB, and Hugues LEROUX

Laboratoire de Structure et Propriétés de l'Etat Solide, Université des Sciences et Technologies de Lille and CNRS,
UMR 8008, F-59655 Villeneuve d'Ascq, France

*Corresponding author. E-mail: julien.stodolna@ed.univ-lille1.fr

(Received 15 May 2009; revision accepted 21 September 2009)

Abstract—Four particles extracted from track 80 at different penetration depths have been studied by analytical transmission electron microscopy (ATEM). Regardless of their positions within the track, the samples present a comparable microstructure made of a silica rich glassy matrix embedding a large number of small Fe-Ni-S inclusions and vesicles. This microstructure is typical of strongly thermally modified particles that were heated and melted during the hypervelocity impact into the aerogel. X-ray intensity maps show that the particles were made of Mg-rich silicates (typically 200 nm in diameter) cemented by a fine-grained matrix enriched in iron sulfide. Bulk compositions of the four particles suggest that the captured dust particle was an aggregate of grains with various iron sulfide fraction and that no extending chemical mixing in the bulb occurred during the deceleration. The bulk S/Fe ratios of the four samples are close to CI and far from the chondritic meteorites from the asteroidal belt, suggesting that the studied particles are compatible with chondritic-porous interplanetary dust particles or with material coming from a large heliocentric distance for escaping the S depletion.

INTRODUCTION

Cometary dust particles are believed to be relicts of the primitive material of the early solar system. Their sojourn in a comet nucleus probably permitted the preservation of primordial signatures from thermal, aqueous or irradiation alterations. For this reason, comets have been targets of a number of recent space missions. Cometary material is now available for studies in the laboratories since the Stardust mission (NASA) brought to Earth samples from the comet 81P/Wild 2 in January 2006. The cometary dust has been collected with a tray composed of low density silica aerogel cells. The particles were stopped in the aerogel at a relative velocity of 6.1 km s^{-1} that caused hypervelocity impacts (Hörz et al. 2006). The deceleration tracks contain cometary material unevenly distributed in various proportions (Hörz et al. 2006; Zolensky et al. 2006; Flynn et al. 2006; Ishii et al. 2008a; Lanzirrotti et al. 2008). This configuration suggests abrasion and ablation or breaking up of the incident particles during the deceleration in the aerogel. For number of samples, in particular those extracted from track walls, the microstructure shows clear evidences of thermal modification in addition to strong intermixing with melted aerogel, showing that the particles suffered thermal alteration during the capture process (Leroux et al. 2008, 2009; Ishii et al. 2008b; Rietmeijer et al. 2008).

The aim of this paper is to compare four particles extracted from the walls of track 80 at various penetration depths. The samples are studied by analytical transmission electron microscopy (ATEM). We compare their relative microstructures and chemical compositions in order to state if the incident particle was homogeneous or made of an assemblage of unrelated subcomponents. We also aimed to increase understanding of the thermal modification process during capture deceleration.

Samples and Analytical Procedure

The allocated samples were prepared at the NASA Johnson Space Center Stardust curatorial facility. The particles were extracted from locations along tracks left in the aerogel using micromanipulators. They are then embedded in EMBED-812 epoxy resin and sliced into $\approx 70 \text{ nm}$ thick sections with an ultramicrotome equipped with a diamond knife. Cut sections are deposited onto C-coated TEM copper grids. Details about extraction and manipulation can be found in Zolensky et al. (2008a). The four particles studied here have been extracted from the walls of the bulb of track 80 (Fig. 1). This track presents a very large bulbous cavity at the entrance and three fine terminal particles emanating out of the bottom of the larger area. Stylus measure is about 4.5 mm in

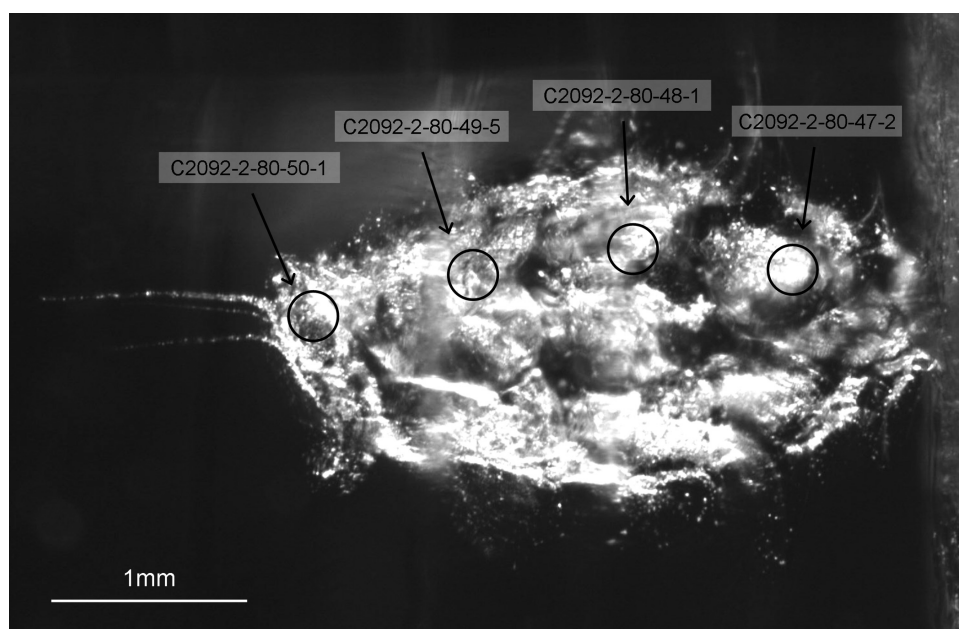


Fig. 1. Localization of the four samples in track 80. The track length is about 4.5 mm and 2 mm in width.

length and 2 mm in width. The studied allocated TEM samples are labeled C2092-2-80-47-2, C2092-2-80-48-1, C2092-2-80-49-5, and C2092-2-80-50-1 (Fig. 2) and correspond respectively to depths 0.8, 1.5, 2.5 and 3.5 mm from the entrance hole.

The samples were studied by ATEM using a Tecnai G2-20 twin (LaB₆ filament, 200kV) equipped with an energy dispersive X-ray spectroscope (EDS) EDAX Si-detector. Grain microstructures were studied by bright- and dark-field imaging in conventional TEM mode and with annular-bright and dark field detectors in scanning (STEM) mode. Compositions were studied by EDS with probe sizes ranging from 5 to 10 nm in the STEM configuration. For quantitative analyses, calculations of element concentrations and atomic ratios were carried out using calibrated *k*-factors and thin film matrix correction procedures. The *k*-factors for the major elements were determined using standard specimens according to the parameter-less method of Van Cappellen (1990). The relative errors are typically 5at% for the major elements (O, Si, Mg, Fe, and S) and 20at% for the minors. Elemental distributions were obtained by EDS X-ray intensity maps, using spectral imaging wherein each pixel of a spectrum image contains a full EDS spectrum. The acquisition time ranged from 15 to 20 hours using drift compensation (see Leroux et al. 2008 for details).

RESULTS

The microstructure of the four samples is quite comparable. It consists of a silica-rich glassy matrix enclosing a large number of small Fe-Ni-S inclusions and vesicles (Fig. 3a). Size of the metal-sulfide droplets is 20 nm

in average and it extends from a few nanometers to one hundred of nanometers. The average abundance is about 100–200 beads per μm^2 for a typically 70 nm thick foil. For the largest Fe-Ni-S inclusions, a metallic Fe-Ni core and a sulfide shell are clearly distinguishable on EDS X-ray intensity maps (Fig. 4). Size of the vesicles is approximately 50 nm in average and they present a lower abundance than the Fe-Ni-S droplets, typically 10 per μm^2 . In general, this microstructure is homogeneous within the sample but locally Fe-Ni-S beads free areas are found (Fig. 3b).

The compositions of the examined grains are highly variable from place to place on a submicron scale. They are all rich in SiO₂ due to a strong impregnation of the incident particle with melted aerogel during the high temperature stage of capture. Consequently the quenched mixture exhibits a low amount of cometary material. Representative compositions are given in Table 1. The major elements are O and Si due to the strong molten aerogel contribution. Mg, Fe and S concentrations are typically within the range 1–3 at%. Some minor elements as Al, Ca, Cr, Mn, and Ni are also present in low proportions, less than 0.5 at%. The fraction of cometary material in the glass has been estimated using the percentage of the major elements Mg, Fe and S, compared to Si and O, assuming that the cometary material have a composition close to CI. Typically this fraction is close to 10%. Table 2 gives a summary of the characteristics of each studied particle, including the size before ultramicrotomy, the analyzed volume by TEM and the percentage of cometary material found in this volume.

In order to compare the chemical composition of the four particles or the variability of composition in a given particle, a Fe-Mg-S ternary representation is well suitable because of

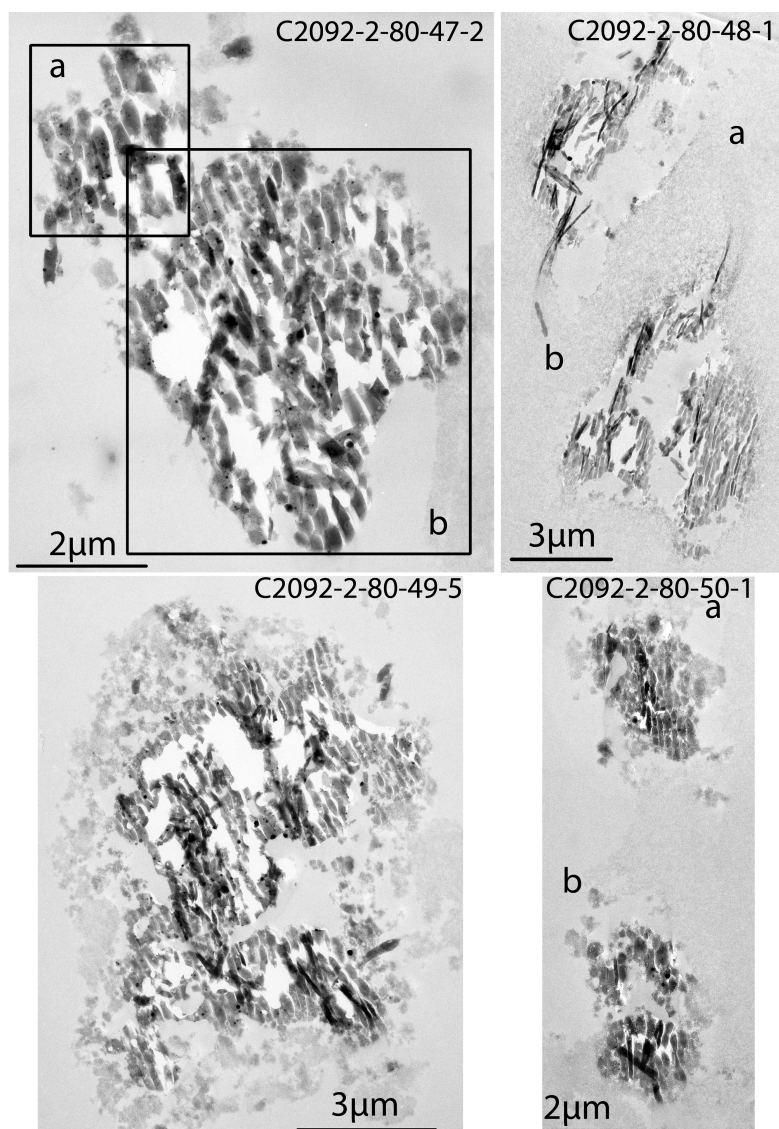


Fig. 2. Bright-field TEM images of entire TEM slices (70 nm thick) of the four studied samples. Some samples present two separate parts reported “a” and “b.”

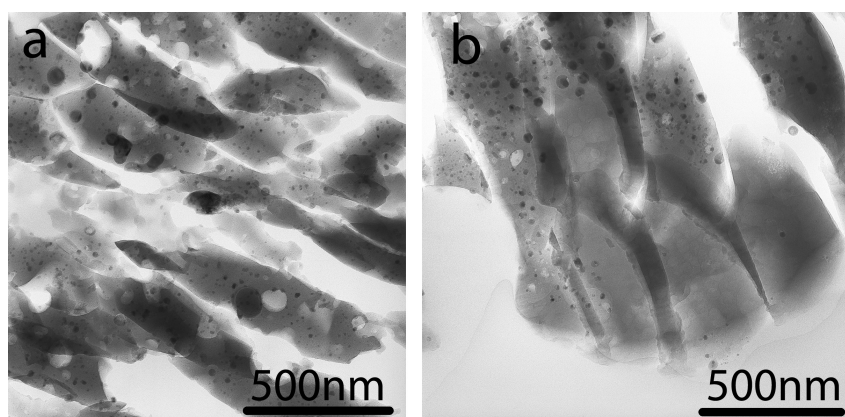


Fig. 3. Bright-field TEM images showing typical microstructure of the silica-rich glassy matrix (a) with and (b) without inclusions and vesicles. The shard-like texture is due to sectioning by ultramicrotomy.

Table 1. Representative EDS compositions (at%) for C2092-2-80-47-2 part 'b'. The $1 \times 1 \mu\text{m}^2$ area compositions were selected randomly and show a low variability. The Mg-rich areas are usually free of Fe-Ni-S nanophases and are Fe-poor, suggesting that the FeO content in the glass is low. The glassy matrix compositions were obtained using small acquisition windows (typically $50 \times 50 \text{ nm}^2$) or point analysis with a probe size 5–10 nm.

O	Si	Fe	S	Mg	Al	Ca	Cr	Mn	Ni
Typical composition $1 \times 1 \mu\text{m}^2$									
65.36	30.95	0.91	1.00	1.06	0.62	0.05	0.02	0.00	0.03
63.36	29.58	2.73	2.13	1.32	0.62	0.11	0.04	0.02	0.08
65.40	29.94	1.23	1.31	1.37	0.58	0.09	0.04	0.01	0.04
64.08	29.80	2.24	1.57	1.44	0.59	0.11	0.02	0.01	0.14
63.94	29.67	1.66	1.48	2.33	0.69	0.12	0.03	0.02	0.06
Mg-rich areas $100 \times 100 \text{ nm}^2$									
63.33	25.85	1.93	1.44	6.31	0.60	0.15	0.05	0.04	0.06
65.94	21.31	0.37	0.39	10.99	0.35	0.13	0.00	0.02	0.00
61.48	22.41	0.45	0.50	13.75	0.57	0.22	0.01	0.01	0.01
Glassy matrix									
64.80	32.70	0.00	0.20	2.10	0.00	0.10	0.10	0.00	0.00
65.50	25.70	0.10	0.70	7.60	0.00	0.40	0.00	0.00	0.00
64.80	29.10	0.30	0.30	4.40	0.40	0.20	0.10	0.20	0.00
Average composition of the Fe-Ni-S nanophases									
–	–	58.19	39.52	–	–	–	–	–	2.29
Bulk									
65.73	28.65	1.36	1.16	2.28	0.61	0.09	0.02	0.01	0.07

Table 2. Characteristics of the four studied particles. The first line is the volume of the particles as extracted by the micromanipulators at JSC. The second line is the volume of material analyzed by ATEM. This corresponds to the surface of the TEM sample multiplied by its thickness. The third line is the percentage of cometary material found in the TEM sections, assuming that the cometary material is close to CI in composition and that the SiO_2 enrichment is due to melted aerogel. Finally, the last line is the deduced original size and volume of the particle before melting with aerogel.

	C2092-2-80-47-2	C2092-2-80-48-1	C2092-2-80-49-5	C2092-2-80-50-1
Volume before ultracut (μm^3)	1800	8000	520	4200
Analyzed volume (μm^3)	3.0	1.7	5.3	0.2
% of refractory material	11	4	11	9
Volume (μm^3)/diameter (μm) before melting and mixing with aerogel	$\approx 200/\approx 7$	$\approx 320/\approx 8.5$	$\approx 60/\approx 5$	$\approx 380/\approx 9$

the molten aerogel admixture (Leroux et al. 2009). The major phases present in extraterrestrial materials such as Fe-Ni metal, Fe-sulfides and Fe-Mg-silicates can be plotted on this diagram and compositions can be compared to those of other already known extraterrestrial objects. In this Fe-Mg-S ternary diagram, the average bulk composition of the samples is shown in Fig. 5. For samples made of two distinct parts (Fig. 2), two different series of measurements have been performed. The average bulk compositions are found slightly enriched in S by comparison with compositions of chondrites, including the CM and the rare K (Kakangari) grouplet (compositions from Wasson and Kallemeyn 1988 and McSween and Richardson 1977). Nevertheless the CI composition is the closest.

The EDS X-ray intensity maps show that distributions of the major elements (Mg, Fe, and S) are relatively homogeneous at the sample scale (Fig. 6). Mg is frequently in good correlation with Fe and S which are dominantly detected in the Fe-Ni-S phases. Locally Mg-rich and

inclusions free areas are detected, which probably correspond to melted Mg-rich silicates precursors, forsterite or enstatite. To study the composition distribution within a given sample, sub-areas compositions have been extracted from the EDS X-ray intensity maps and plotted in the ternary Fe-Mg-S diagram. Figure 7 shows compositions extracted from $400 \times 400 \text{ nm}^2$ sub-areas which were randomly selected over the sample. Each area corresponds to a low amount of cometary material, approximately $1.5 \times 10^{-3} \mu\text{m}^3$. The almost pure SiO_2 areas, containing less than 1% of non SiO_2 analysed material, were discarded. On the Fe-Mg-S diagram, the compositions are scattered along a line joining approximately the Mg corner and the average composition of the Fe-Ni-S phases. The S/Fe and Ni/Fe ratios are close to 0.85 and 0.05, respectively (Table 1). The silica-rich glassy matrix compositions are given in Table 1 and plotted in the ternary Fe-Mg-S diagram in Fig. 8, together with the average composition of the Fe-Ni-S nanophases which are quite comparable from sample to

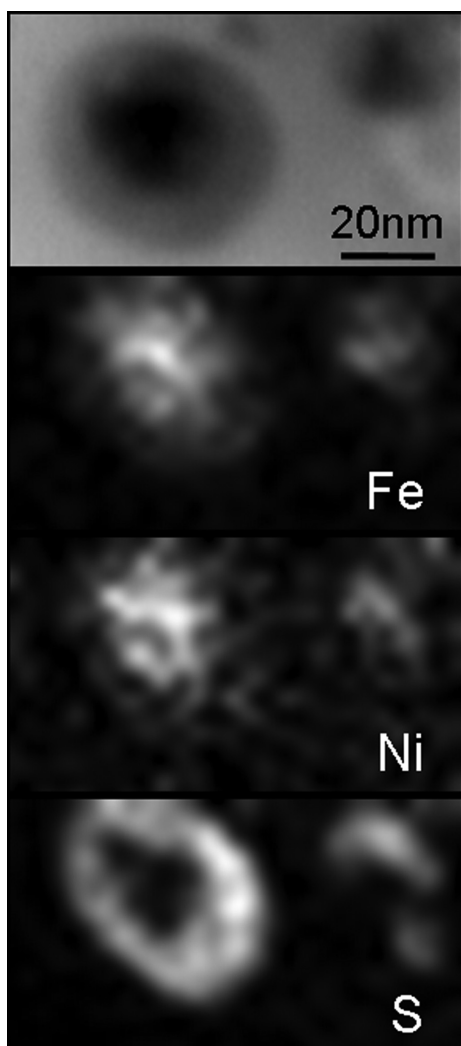


Fig. 4. Bright-field STEM image and EDS elemental distribution for Fe, Ni, and S of a Fe-Ni-S inclusion. A metallic Fe-Ni core and a sulfide shell are clearly distinguishable.

sample. The matrix composition is highly variable from place to place but the Fe concentration is always very low compared to the bulk composition. Each sample also contains Mg-rich patches, as seen for instance in Fig. 6. Corresponding representative compositions are given in Table 1. These compositions are also plotted in Fig. 9 together with compositions of sub-areas without these Mg-rich patches. This distribution of the elements in the glassy matrix strongly suggests that the cometary material was constituted by a fine-grained sulfide-rich component and Mg-rich silicates typically several hundreds of nanometers. By surface measurements on the X-rays intensity maps and with the corresponding compositions of each components (Mg-rich and sulfide-rich background), the relative fraction has been estimated. The Mg-rich material represents about 0.09 to 0.15 at% of the particles. Table 3 summarized the main chemical characteristics for the four samples.

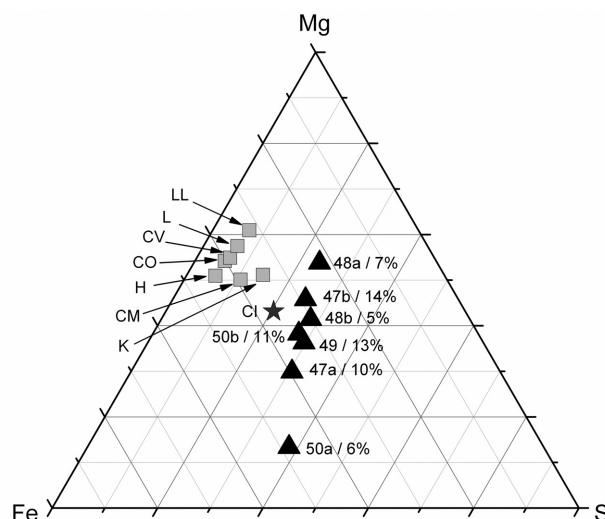


Fig. 5. Average compositions of the four samples in the ternary Fe-Mg-S diagram (carbonaceous and ordinary chondrites compositions from Wasson and Kallemeyn 1988 and K chondrite from McSween and Richardson 1977). Some samples present two separate parts with distinct average compositions (a and b). The weight of each composition is reported close to each point. It corresponds to the product of the percentage of cometary material found in the TEM section with the volume of the sample.

DISCUSSION

Track 80 is a bulbous type B track where several small styli emerge beneath the main cavity. This configuration suggests the impact of a highly porous aggregate made of a mixture of fine-grained materials containing coarse components (Hörz et al. 2006; Burchell et al. 2008; Trigo-Rodríguez et al. 2008). The original particle size and mass can be estimated with the assumptions that the track volume is related to the incident kinetic energy and that the diameter of the entrance hole is related to the size of the particle (Burchell et al. 2008). The track volume is close to 7 mm^3 . According to the calibration curve by Burchell et al. (2008), the corresponding kinetic energy is about $15 \pm 4 \text{ mJ}$. With an impact speed of 6.1 km s^{-1} the impactor mass is $6.4 \pm 1.6 \times 10^{-10} \text{ kg}$. The entrance hole diameter is 410 microns, corresponding to a particle diameter of about 70 microns, this latter value is being deduced with a large uncertainty. The deduced density is thus about $4000 \pm 2000 \text{ kg m}^{-3}$ which appears a little high for a porous aggregate. The four studied samples correspond to fragments disrupted and left along the track into the aerogel. The average concentration of the cometary material in the slices and the size of the extracted particles before the sectioning by ultramicrotomy allow an estimate of the size of the fragment before melting with aerogel (Table 2). The fragments correspond to spheres with diameters between 5 and $10 \text{ }\mu\text{m}$. These four samples represent less than 1% of the parent particle which impacted the aerogel. This low proportion confirms that the parent particle broke up and dispersed its components into the track volume.

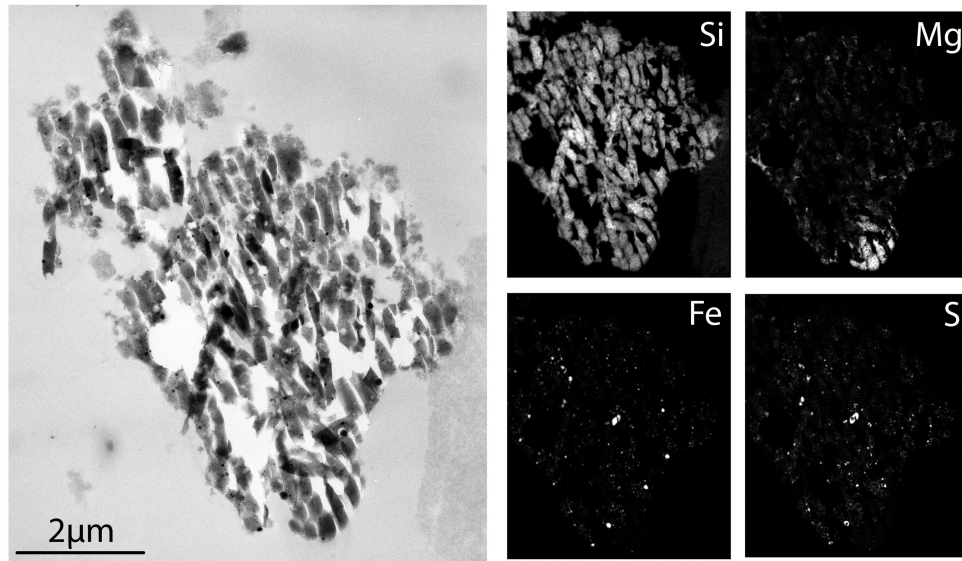


Fig. 6. Bright-field STEM image and EDS elemental distributions for Si, Mg, Fe and S in the part 'b' of the sample C2092-2-80-47-2. Fe, S localized in the Fe-Ni-S beads and Mg are frequently in good correlation. Locally Mg rich areas free of beads are observed.

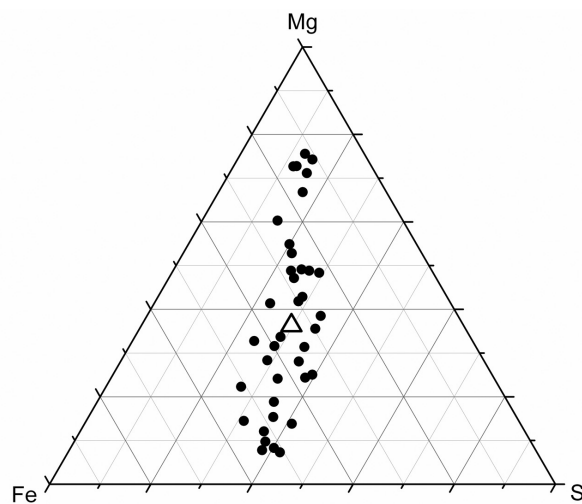


Fig. 7. Bulk (triangle) and sub-areas (disk) compositions of C2092-2-80-49-5 plotted in a Fe-Mg-S ternary diagram. Each sub-areas composition represents an analyzed volume about $1.5 \times 10^{-3} \mu\text{m}^3$.

Table 3. Main chemical characteristics of the four studied particles, including the fraction of the Mg-rich patches versus the sulfide-rich fine grained material and the S/Fe of the samples.

	C2092-2-80-47-2	C2092-2-80-48-1	C2092-2-80-49-5	C2092-2-80-50-1
Fraction of Mg-rich patches	0.11	0.09	0.14	0.15
S/Fe ratio	0.84	0.89	0.88	0.84

The particles show clear evidence for melting and mixing with molten aerogel. This is typical of strongly altered particles which are frequently found in dust extracted from

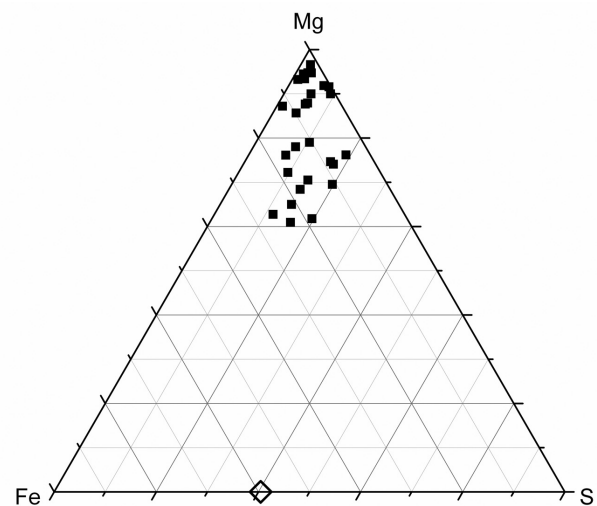


Fig. 8. Representative composition of the silica rich glassy matrix of the four samples (black filled square). These compositions have been measured by spot analysis (electron beam diameter 5–10 nm) between the Fe-Ni-S inclusions. The white diamond represents the average composition of the Fe-Ni-S nanophases.

Stardust track in aerogel (Leroux et al. 2008; Zolensky et al. 2008b). In the ternary Fe-Mg-S diagrams, the compositions are distributed along a line which joins the Mg corner and the average Fe/S relative composition of the Fe-Ni-S nanophases. This line represents a constant Fe/S ratio, suggesting that all the iron is contained in Fe-Ni-S nanophases and that the silica-rich glassy matrix is depleted in FeO, as confirmed by spot analyses (Table 1 and Fig. 8). This configuration agrees with results from Leroux et al. (2009) who proposed a Fe-Ni-S nanophase formation model based on a reduction reaction process that happened during the high temperature stage of

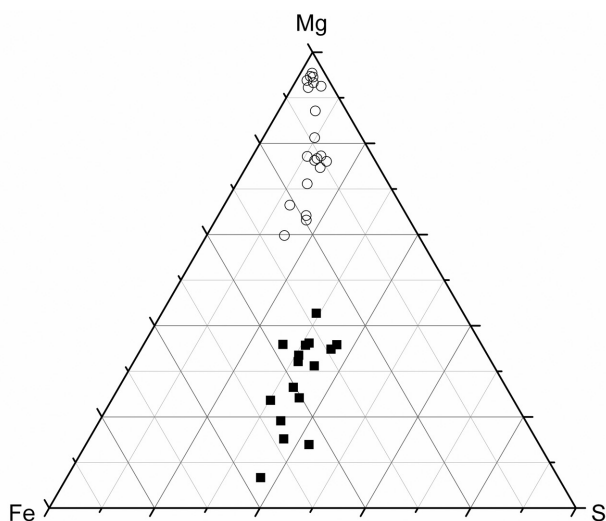


Fig. 9. Composition of the Mg-rich patches of the four samples (white open disk) and of the fine grained material (black filled squares). These compositions have been measured using the X-rays intensity maps in order to localize the Mg rich areas. The volume of analysis is variable for each plotted composition.

the capture. The reduction occurred between the FeO-bearing silicates and the carbonaceous matter coming from either the incoming particles or residual organics in the aerogel. This model also includes thermal decomposition of indigenous sulfides, redistribution of gaseous S_2 and further condensation on iron beads during cooling (Fig. 4). Iron reduction was also reported by Marcus et al. (2008) and Westphal et al. (2009).

The four samples suffered from thermal modification at comparable level, whatever their position in the bulbous region of the track. However, the extracted particles studied here have clear distinct bulk composition (Fig. 5), even when two particles are found in the same sample and are thus spatially very close (less than $5 \mu\text{m}$ for particles 48 and 50). Chemical mixing during the capture heating in the track, if it occurs, was spatially very limited. Variable compositions are probably due to variation in the relative proportion of silicate and iron-sulfide in the individual pieces of the initial aggregate which broke up during the hypervelocity impact. The X-ray intensity chemical maps revealed that the studied samples have a bimodal nature. They contain relatively large Mg-rich patches and a background with a relatively low concentration of Fe, Mg, and S as major elements. This configuration suggests that the incident fragments were made of Mg-rich silicate nuggets (ranging from 200 nm to $1 \mu\text{m}$ in diameter) stick together with a very fine-grained material enriched in Fe and S. From the elemental X-ray intensity maps, we have estimated the relative proportion of these two components in the different samples studied (Table 3). We found that the Mg-silicates fraction range from 0.09 to 0.15.

All studied samples show compositions enriched in Fe and S compared to the CI composition (Fig. 5). The deduced average elemental S/Fe ratio is close to 0.85. Table 3 gives

this ratio for the four studied samples. This ratio is higher than the CI value, which is equal to 0.56, according to the recommended element abundance by Wasson and Kallemeyn (1988). This ratio normalized to CI is $S/Fe = 1.5 \times CI$. This value strongly differs from the bulk analysis of tracks by Flynn et al. (2006) which reported a significant S underabundance, as measured by synchrotron X-ray microprobes (SXR). Note that the authors also pointed out that the S value was underestimated in the fluorescence measurements because of the strong absorption of the S $K\alpha$ X-rays in the aerogel. In contrast to SXR, our S/Fe estimation is made on extracted particles and the corresponding amount of material analyzed is very low compared to synchrotron measurements. However, the four samples raise comparable S/Fe values and thus are considered as reasonably representative of the whole incident particle which generated the track 80. In a recent study, Westphal et al. (2009) deduced S/Fe ratios in several tracks by using the Fe $K\alpha$ X-rays, the sulfide fraction being deduced from the X-ray absorption near-edge structure (XANES). They found an average S/Fe ratio = 0.46, which is very close to CI. Comparable values were also deduced by EDS-TEM measurements on thermally modified material extracted from different tracks by Leroux et al. (2008, 2009). A CI-like composition is also supported by TOF-SIMS analyses (Stephan et al. 2008a, 2008b) and is also suggested by the distribution of olivine compositions in Wild 2 grains (Zolensky et al. 2008b).

CONCLUSION

The ATEM study of four particles from track 80 shows intensive melting and mixing with melted aerogel. Elemental X-ray intensity maps reveal that the particles were constituted by an assemblage of Mg-rich silicates, typically 200 nm to $1 \mu\text{m}$ in size cemented by a sulfide-rich fine-grained material. The bulk average composition shows a high S/F ratio, approximately $1.5 \times CI$. These Wild 2 particles are comparable in bulk chemistry and in fine-grained arrangement to anhydrous chondritic porous interplanetary dust particles. The high S/Fe ratio is found far from the composition field of other meteorite groups which are depleted in S by a factor of 3–5 with respect to CI. This Wild 2 material likely originated from a large heliocentric distance for escaping the S depletion.

Acknowledgments—K. Nakamura-Messenger is gratefully acknowledged for the preparation of ultramicrotomed TEM samples. We thank M. Burchell for discussion about track morphology. We thank support by Centre National d'Etudes Spatiales (CNES) and the electron microscope facility by CNRS (INSU), European FEDER and region Nord-Pas-de-Calais. We also thank J. F. Dhenin and A. Addad for their help with the TEM and M. Zolensky for a detailed review and constructive comments on the manuscript.

Editorial Handling—Dr. Anthony Jones

REFERENCES

- Burchell M. J., Fairey S. A. J., Wozniakiewicz P., Brownlee D. E., Hörz F., Kearsley A. T., See T. H., Tsou P., Westphal A., Green S. F., Trigo-Rodríguez J. M., and Dominguez G. 2008. Characteristics of cometary dust tracks in Stardust aerogel and laboratory calibrations. *Meteoritics & Planetary Science* 43:23–40.
- Flynn G. J., Bleuet P., Borg J., Bradley J. P., Brenker F. E., Brennan S., Bridges J., Brownlee D. E., Bullock E. S., Burghammer M., Clark B. C., Dai Z. R., Daghlian C. P., Djouadi Z., Fakra S., Ferroir T., Floss C., Franchi I. A., Gainsforth Z., Gallien J.-P., Gillet Ph., Grant P. G., Graham G. A., Green S. F., Grossemey F., Heck P. R., Herzog G. F., Hoppe P., Hörz F., Huth J., Ignatyev K., Ishii H. A., Janssens K., Joswiak D., Kearsley A. T., Khodja H., Lanzirrotti A., Leitner J., Lemelle L., Leroux H., Luening K., MacPherson G. J., Marhas K. K., Marcus M. A., Matrajt G., Nakamura T., Nakamura-Messenger K., Nakano T., Newville M., Papanastassiou D. A., Pianetta P., Rao W., Riekel C., Rietmeijer F. J. M., Rost D., Schwandt C. S., See T. H., Sheffield-Parker J., Simionovici A., Sitnitsky I., Snead C. J., Stadermann F. J., Stephan T., Stroud R. M., Susini J., Suzuki Y., Sutton S. R., Taylor S., Teslich N., Troadec D., Tsou P., Tsuchiyama A., Uesugi K., Vekemans B., Vicenzi E. P., Vincze L., Westphal A. J., Wozniakiewicz P., Zinner E., and Zolensky M. E. 2006. Elemental compositions of comet 81P/Wild 2 samples collected by Stardust. *Science* 314:1731–1735.
- Hörz F., Bastien R., Borg J., Bradley J. P., Bridges J. C., Brownlee D. E., Burchell M. J., Chi M., Cintala M. J., Dai Z. R., Djouadi Z., Dominguez G., Economou T. E., Fairey S. A. J., Floss C., Franchi I. A., Graham G. A., Green S. F., Heck P., Hoppe P., Huth J., Ishii H., Kearsley A. T., Kissel J., Leitner J., Leroux H., Marhas K., Messenger K., Schwandt C. S., See T. H., Snead C., Stadermann F. J., Stephan T., Stroud R., Teslich N., Trigo-Rodríguez J. M., Tuzzolino A. J., Troadec D., Tsou P., Warren J., Westphal A., Wozniakiewicz P., Wright I., and Zinner E. 2006. Impact features on Stardust: Implications for comet 81P/Wild 2 dust. *Science* 314:1716–1719.
- Ishii H. A., Brennan S., Bradley J. P., Luening K., Ignatyev K., and Pianetta P. 2008a. Recovering the elemental composition of comet Wild 2 dust in five Stardust impact tracks and terminal particles in aerogel. *Meteoritics & Planetary Science* 43:215–231.
- Ishii H. A., Bradley J. P., Dai Z. R., Chi M., Kearsley A. T., Burchell M. J., Browning N. D., and Molster F. 2008b. Comparison of comet 81P/Wild 2 Dust with interplanetary dust from comets. *Science* 319:447–450.
- Lanzirrotti A., Sutton S. R., Flynn G. J., Newville M., and Rao W. 2008. Chemical composition and heterogeneity of Wild 2 cometary particles determined by synchrotron X-ray fluorescence. *Meteoritics & Planetary Science* 43:187–213.
- Leroux H., Rietmeijer F. J. M., Velbel M. A., Brearley A. J., Jacob D., Langenhorst F., Bridges J. C., Zega T. J., Stroud R. M., Cordier P., Harvey R. P., Lee M., Gounelle M., and Zolensky M. E. 2008. A TEM study of thermally modified Comet 81P/Wild 2 dust particles by interactions with the aerogel matrix during the Stardust capture process. *Meteoritics & Planetary Science* 43:97–120.
- Leroux H., Roskosz M., and Jacob D. 2009. Oxidation state of iron and extensive redistribution of sulfur in thermally modified Stardust particles. *Geochimica et Cosmochimica Acta* 73:767–777.
- Marcus M. A., Fakra S., Westphal A. J., Snead C. J., Keller L. P., Kearsley A., and Burchell M. J. 2008. Smelting of Fe-bearing glass during hypervelocity capture in aerogel. *Meteoritics & Planetary Science* 43:87–96.
- McSween H. Y. and Richardson S. M. 1977. The composition of carbonaceous chondrite matrix. *Geochimica et Cosmochimica Acta* 41:1145–1161.
- Rietmeijer F. J. M., Nakamura T., Tsuchiyama A., Uesugi K., Nakano T., and Leroux H. 2008. Origin and formation of iron-silicide phases in the aerogel of the Stardust mission. *Meteoritics & Planetary Science* 43:121–134.
- Stephan T., Flynn G. J., Sandford S. A., and Zolensky M. E. 2008a. TOF-SIMS analysis of cometary particles extracted from Stardust aerogel. *Meteoritics & Planetary Science* 43:285–298.
- Stephan T., Rost D., Vicenzi E. P., Bullock E. S., MacPherson G. J., Westphal A. J., Snead C. J., Flynn G. J., Sandford S. A., and Zolensky M. E. 2008b. TOF-SIMS analysis of cometary matter in Stardust aerogel tracks. *Meteoritics & Planetary Science* 43:233–246.
- Trigo-Rodríguez J. M., Dominguez G., Burchell M. J., Hörz F., and Llorca J. 2008. Bulbous tracks arising from hypervelocity capture in aerogel. *Meteoritics & Planetary Science* 43:75–86.
- Van Cappellen E. 1990. The parameterless correction method in X-ray microanalysis. *Microscopy Microanalysis Microstructures* 1:1–22.
- Wasson J. T. and Kallemeyn G. W. 1988. Composition of chondrites. *Philosophical Transactions of the Royal Society of London A* 325:535–544.
- Westphal A. J., Fakra S. C., Gainsforth Z., Marcus M. A., Ogliore R. C., and Butterworth A. L. 2009. Mixing Fraction of Inner Solar System Material in Comet 81P/Wild 2. *The Astrophysical Journal* 591:18–28.
- Zolensky M. E., Zega T. J., Yano H., Wirick S., Westphal A. J., Weisberg M. K., Weber I., Warren J. L., Velbel M. A., Tsuchiyama A., Tsou P., Toppani A., Tomioka N., Tomeoka K., Teslich N., Taheri M., Susini J., Stroud R., Stephan T., Stadermann F. J., Snead C. J., Simon S. B., Simionovici A., See T. H., Robert F., Rietmeijer F. J. M., Rao W., Perronnet M. C., Papanastassiou D. A., Okudaira K., Ohsumi K., Ohnishi I., Nakamura-Messenger K., Nakamura T., Mostefaoui S., Mikouchi T., Meibom A., Matrajt G., Marcus M. A., Leroux H., Lemelle L., Le L., Lanzirrotti A., Langenhorst F., Krot A. N., Keller L. P., Kearsley A. T., Joswiak D., Jacob D., Ishii H., Harvey R., Hagiya K., Grossman L., Grossman J. N., Graham G. A., Gounelle M., Gillet Ph., Genge M. J., Flynn G., Ferroir T., Fallon S., Ebel D. S., Dai Z. R., Cordier P., Clark B., Chi M., Butterworth A. L., Brownlee D. E., Bridges J. C., Brennan S., Brearley A., Bradley J. P., Bleuet P., Bland P. A., and Bastien R. 2006. Mineralogy and petrology of comet 81P/Wild 2 nucleus samples. *Science* 314:1735–1739.
- Zolensky M. E., Nakamura-Messenger K., Fletcher L., and See T. 2008a. Curation, spacecraft recovery, and preliminary examination for the Stardust mission: A perspective from the curatorial facility. *Meteoritics & Planetary Science* 43:5–21.
- Zolensky M., Nakamura-Messenger K., Rietmeijer F., Leroux H., Mikouchi T., Ohsumi K., Simon S., Grossman L., Stephan T., Weisberg M., Velbel M., Zega T., Stroud R., Tomeoka K., Ohnishi I., Tomioka N., Nakamura T., Matrajt G., Joswiak D., Brownlee D., Langenhorst F., Krot A., Kearsley A., Ishii H., Graham G., Dai Z. R., Chi M., Bradley J., Hagiya K., Gounelle M. and Bridges J. 2008b. Comparing Wild 2 particles to chondrites and IDPs. *Meteoritics & Planetary Science* 43:261–272.